The Influence of Land Surface Properties on Sahel Climate. Part II: Afforestation

YONGKANG XUE AND JAGADISH SHUKLA

Center for Ocean–Land–Atmosphere Studies, Institute of Global Environment and Society, Calverton, Maryland

(Manuscript received 8 June 1993, in final form 19 August 1994)

ABSTRACT

A numerical experiment was performed to explore the nature of and mechanisms for the effect of large-scale afforestation in the sub-Saharan area on the climate. This sensitivity study, which consists of several short-term integrations of a climate model, suggests that afforestation would enhance the rainfall in the region and would have the largest impact during dry years. While the rainfall increased in the afforestation area, it decreased to the south of that region. It was found that this land surface change altered the surface energy balance and induced a circulation change that led to a change in rainfall. The influences of different vegetation species and the extent of the afforestation area on the rainfall were tested and are discussed. Reducing the afforestation area by about 50% still resulted in a positive simulated rainfall anomaly. A detailed analysis of the surface energy balance is presented. A comparison between the effects of afforestation and desertification is also made.

1. Introduction

It has been recognized that land surface changes may affect regional climate variations over a wide range of timescales. A previous study (Xue and Shukla 1993) demonstrated the large impact of desertification on the Sahelian summer circulation. In this paper, the effects of large-scale afforestation in the sub-Saharan region are investigated. Since this marginal region has frequently experienced drought in the past, a number of schemes have been proposed to augment precipitation by changing surface conditions there. As early as the 1920s, an ambitious water regulation project was proposed by German civil engineer H. Sergel to divert the water of the Congo River into the Chad Basin (Flohn et al. 1974). This project was designed to supply irrigation water for part of the Sahara. It was also expected that there would be more evaporation from the wet surface. However, according to Flohn's rough estimation, diversion of the Congo River into Lake Chad might increase the rainfall there by only 10%, which is not very useful considering the high interannual rainfall variability in that region. Similar schemes, which suggested developing large inland bodies of water in and around the Sahara, were also questioned because the deficiency of rain during the sub-Saharan summer is caused mainly by dynamical factors, that is, by large-scale subsidence in this region (Flohn et al. 1974). To enhance vertical motion and, hence, convective precipitation, Black and Tarmy (1963) suggested creating asphalt islands in semiarid regions. They expected that the low surface albedo of the asphalt surface would increase the surface temperature and create a thermal ridge, which could promote cloud formation and rainfall. Despite the low investment cost as compared to other project costs, the negative environmental consequences of Black's plan and political considerations have prevented it from being applied (Glantz 1977). Another plan, which involved planting a forest belt in West Africa to combat desertification, was proposed by Stebbing (1938). He expected this belt to stop the sands from moving southward, break up the northeast hot dry wind, and encourage moisture retention in the soil. Before the 1970s, this plan was not considered as a weather and climate modification scheme because a majority of scientists believed that in arid zones afforestation could not have any significant effect on the regional climates (Le Houerou 1977).

Despite the controversy, combating desertification through afforestation has actually been practiced in Africa for many years (FAO 1989). The United Nations and several countries have launched campaigns to combat desertification. One of the important aspects of these efforts is revegetating denuded areas. As far as we know, these ideas have not been tested in any general circulation model owing to the simplicity of the treatment of vegetation in GCMs and the coarse resolution of the models. Previous afforestation proposals have been based mainly upon the ideas that afforestation would aid in maintaining the soil and water base for food production, preventing erosion, and breaking up the dry northeast wind. Since drought conditions in the sub-Sahara arise mainly from large-scale motion, it is imperative to examine the impact of afforestation on the large-scale circulation and rainfall for the sub-Sa-

Corresponding author address: Dr. Yongkang Xue, Center for Ocean–Land–Atmosphere Studies, 4041 Powder Mill Road, Suite 302, Calverton, MD 20705-3106.

TABLE 1. Initial and boundary conditions used in the model integrations.

Case	Initial condition	SST boundary condition	Land surface conditions in the test area	Types
C1	1 June 1988	climatology	shrubs with bare soil and shrubs with ground cover	8, 9
C2	2 June 1988	climatology	shrubs with bare soil and shrubs with ground cover	8, 9
C3	1 June 1987	climatology	shrubs with bare soil and shrubs with ground cover	8, 9
C4	1 June 1988	1983 SST	shrubs with bare soil and shrubs with ground cover	8, 9
C5	1 June 1988	1950 SST	shrubs with bare soil and shrubs with ground cover	8, 9
R1	1 June 1988	climatology	afforestation using broadleaf trees with ground cover	6
R2	2 June 1988	climatology	afforestation using broadleaf trees with ground cover	6
R3	1 June 1987	climatology	afforestation using broadleaf trees with ground cover	6
R4	1 June 1988	1983 SST	afforestation using broadleaf trees with ground cover	6
R5	1 June 1988	1950 SST	afforestation using broadleaf trees with ground cover	6
R32	1 June 1987	climatology	afforestation using broadleaf deciduous trees	2
RS1	1 June 1988	climatology	afforestation using broadleaf deciduous trees in small area	2
RS2	2 June 1988	climatology	afforestation using broadleaf deciduous trees in small area	2
RS3	1 June 1987	climatology	afforestation using broadleaf deciduous trees in small area	2

haran region and the mechanisms of land–atmosphere interaction through GCM experiments.

Since the mid 1970s a number of numerical experiments have shown that rainfall increases with an increase in vegetation and soil moisture and a decrease in surface albedo (Charney 1975; Shukla and Mintz 1982; Anthes 1984; Xue et al. 1990). In this study we have used a high resolution model of the global atmosphere and a realistic model of the global biosphere (SSiB, Xue et al. 1991), which is a simplified version of the Simple Biosphere Model (SiB) of Sellers et al. (1986), to investigate the effects of afforestation on the Sahel climate. As a first step, we have designed a hypothetical sensitivity experiment in which we changed the land surface conditions in a large part of the sub-Saharan region from desert and shrubs to broadleaf trees with shrubs. We felt that, if a substantial change over a large area did not make any significant impact in precipitation, further study with changes in small regions might be in vain. In this study we have focused more on the impact and mechanisms of land surface change on climate than on more practical problems such as the most economic scales and the best vegetation species for afforestation, although this is discussed briefly later in this paper. In section 2 we present the design of the afforestation scenarios. The results from numerical experiments are discussed in sections 3 and 4. Section 3 discusses the impact of afforestation on rainfall and its interaction with large-scale circulation, and section 4 shows the surface energy balance. The results are discussed in section 5 and summarized in section 6.

2. Experimental design of the afforestation experiment

The COLA GCM with a simplified vegetation model (SSiB) was used for this study. In SSiB for a vegetated surface, both the canopy and bare soil contribute to evaporation. Evaporation from the canopy includes transpiration and direct re-evaporation from intercepted precipitation. The parameterization for radiative transfer includes consideration of interception, transmission, and absorption of radiation by vegetation and multiple reflections between vegetation and soil. The models and control experiment design have been described in Part I (Xue and Shukla 1993) and will not be discussed here. The five afforestation cases in this experiment were paired with five control cases. Each afforestation case had the same initial condition and sea surface temperature as the corresponding control case. However, the land surface conditions in the sub-Saharan region were different: vegetation types and soil textures were changed in the afforestation experiment. The five control cases (referred to as C1, C2, C3, C4, and C5) and five afforestation cases (R1, R2, R3, R4, and R5) are listed in Table 1. (The other experiments listed in this table are explained later.) Among the ten cases, C1, C2, C3, R1, R2, and R3 used climatological SST as a boundary condition globally. Cases C4 and R4 used 1983 SST, and C5 and R5 used 1950 SST.

Based on past empirical investigations and numerical simulations, a relationship between SST variations and sub-Saharan rainfall is well established. (Lamb 1978; Lamb and Peppler 1991; Folland et al. 1986, 1991; Semazzi et al. 1988.) In this paper we do not address the question of the effects of SST on Sahel climate. The reason that 1983 and 1950 SST boundary conditions were chosen was to investigate the effects of afforestation on a variety of mean climates. For example, 1983 was a very dry year in the Sahel and 1950 was very wet. The COLA GCM successfully simulates the rainfall difference using appropriate SSTs. In this study, the same SST was used in each pair, both for the control and afforestation case so that the difference between the two integrations of each pair could be attributed to the afforestation. Since we are interested in the impact of afforestation on a variety of mean conditions, it would be better to have a multiyear integration with different SSTs. The reasons why we chose seasonal

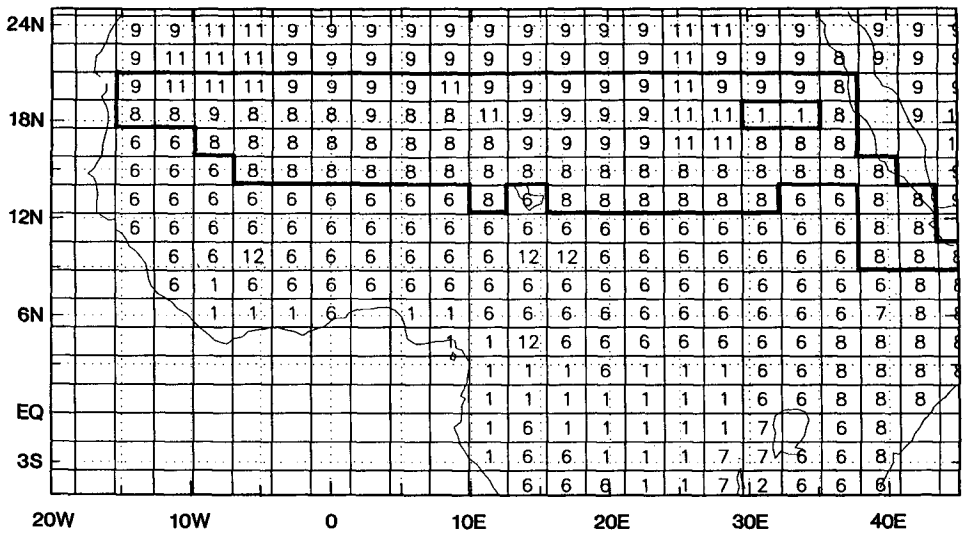

FIG. 1. Vegetation type map of the sub-Saharan region for the control run. Type 1 is tropical rainforest. Type 2 is broadleaf deciduous trees. Type 6 is broadleaf trees with ground cover. Type 7 is grassland. Type 8 is broadleaf shrubs with ground cover. Type 9 is shrubs with bare soil. Type 11 is bare soil. Type 12 is crops. The test area is enclosed by the bold line. For the afforestation experiment all grid points in the test area except type 1 are changed to type 6.

integrations are because of the well-defined rainy season in the Sahel and the limitations of available computer time. We consider this approach better than using only one SST (climatological SST) for each pair of experiments. The averages of five afforestation and control cases will be referred to as experiment R and experiment C, respectively, and the five-case mean of the desertification experiment will be referred to as experiment D. We integrated each case for 90 days from 1 June in four cases and 2 June in the other and computed three-month averages. The differences between each pair of afforestation and control integrations were interpreted as the impact of afforestation.

The area with surface condition changes, referred to as the test area, extends from 13° to 20°N and is enclosed by the bold lines in Fig. 1, which is a map of North African vegetation types used in our GCM. All the grid points with vegetation type 8 (shrubs with ground cover), type 9 (shrubs with bare soil), and type 11 (bare soil) were replaced by vegetation type 6 (broadleaf trees with ground cover) in the afforestation integrations. The values of some vegetation and soil parameters for these types are shown in Table 2. These morphological, physiological, and physical parameters have been discussed in detail in Dorman and Sellers (1989). The vegetation cover, leaf area index, and surface roughness length were substantially increased in the afforestation experiment. The percentage of trees in the afforestation area was increased by 0.2, and the total leaf area index in the test area was increased by more than 2.5 compared with types 8 and 9. The soil type was changed from sandy to loam. The albedos in experiment R were decreased by about 0.10 and 0.12 in the test area originally covered by type 9 and 11,

TABLE 2. Vegetation parameters for five vegetation types.

	Type 2 (broadleaf deciduous trees)	Type 6 (broadleaf trees with ground cover)	Type 8 (shrubs with ground cover)	Type 9 (shrubs with bare soil)	Type 11 (bare soil)
Three-month mean albedo	0.14	0.20	0.21	0.30	0.32
Initial soil wetness in test area	0.17	0.16	0.05	0.05	0.05
Three-month mean roughness length (m)	1.04	0.90	0.22	0.06	0.01
Depth of three soil layers (m)					
$z1$	0.02	0.02	0.02	0.02	0.02
$z2$	1.48	1.48	0.47	0.47	0.17
$z3$	2	2	1	1	0.3
Vegetation cover	0.75	0.3	0.1	0.1	0
Three-month mean leaf area index	5.11	3.08	0.44	0.21	0

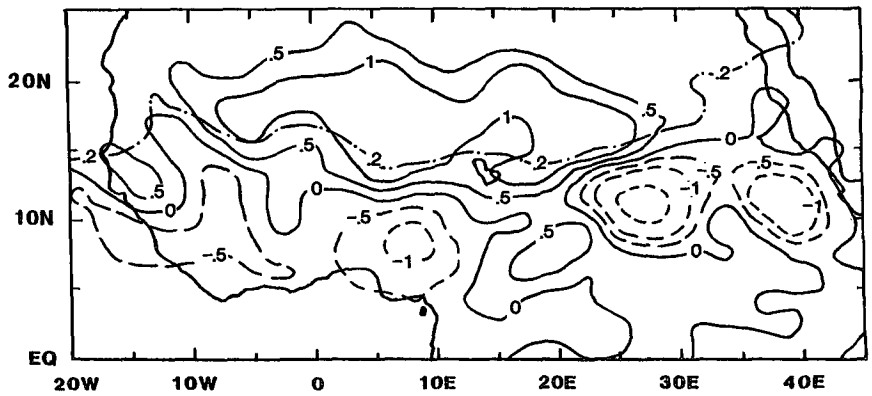

FIG. 2. Three-month mean rainfall differences (afforestation − control). Contours are −8, −4, −2, −1, −0.5, 0, 0.5, 1, 2, 4, and 8 mm/day.

respectively. Since type 8 and type 6 have almost the same values of albedo, only the northern part of the test area exhibits increased albedo.

The initial soil wetness in each experiment is defined by a procedure described by Sato et al. (1989). It is derived from a seasonally varying climatological soil moisture (Mintz and Serafini 1984) using a procedure that is dependent on the vegetation type. Since the water holding capacity, vegetation cover, surface resistance, and other surface properties differ for different vegetation types, this procedure will produce different values of initial soil wetness from the same climatological soil moisture for different vegetation types. Therefore, the initial soil wetness in the test area was different in the afforestation experiment. The initial soil moisture changes in this experiment appear to be consistent with the vegetation type changes. It is shown in section 3 that the evaporation in the control and the afforestation experiments is quite similar during the first few days of integration.

It is recognized that model-simulated climate, in some cases, can take longer than a season to reach equilibrium, and a multiyear integration may be desirable. However, useful conclusions can also be drawn from several short integrations. We chose to make five pairs of seasonal integrations in this study. There are several reasons for this: it is not the equilibrium climate itself that interests us. We are merely interested in the difference between the two climates. This implies an assumption of similar climate drift between the two experiments, which is removed when we subtract the control from the afforestation experiment. The Sahel region has a well-defined rainy season, and we are interested in studying the impact of afforestation on a variety of mean conditions. We believe that by repeating the major experiment five times with different initial and boundary conditions, we have increased the reliability of our results. Although this approach is not the same as running a model for many years, it does provide more information for assessing the results with available computer time.

3. The impact of afforestation on rainfall and circulation

For each case the model was integrated for 3 months from June to August. Figure 2a, which depicts the differences in the 3-month mean rainfall between experiments R and C, shows that the rainfall is augmented in most afforestation areas but reduced to the south of those areas. The 3-month mean rainfall in experiment R, averaged over the test area, increased by 0.8 mm/day, which was 27% more than in the control run. Since the location where the surface conditions were changed was close to the descending branch of the tropical Hadley circulation, the rainfall in the control experiment in this region was small. However, in most of the test area, the rainfall increased by more than 20%. The area north of the dashed–dotted line in Fig. 2a had more than a 20% increase. Meanwhile, the reduction in rainfall to the south of the test area was less than 10% in most places. From the zonally averaged 3-month mean rainfall, we found that the axis of maximum rainfall did not shift in R and the rainfall simply increased in the test area and decreased to the south of this region. The precipitation in the model is produced from both large-scale condensation and deep convection. The changes in model-simulated rainfall were mainly caused by changes in convective activity.

Figure 2 further shows that in this experiment rainfall increased significantly in the central region of the test area. It did not increase much over some parts of the afforestation area. In the eastern part in particular, the rainfall increase did not occur east of 30°E during the entire integration period despite being an afforestation area. This in turn reduced the mean rainfall increase averaged over the entire test area. If we exclude the area east of 30°E, the rainfall in R increased by 1.1 mm/day, about 34% more than the control run.

The rainfall anomaly during the three-month integration was not uniform. Figure 3 shows the time series of the rainfall anomaly in experiment R, which is zon-

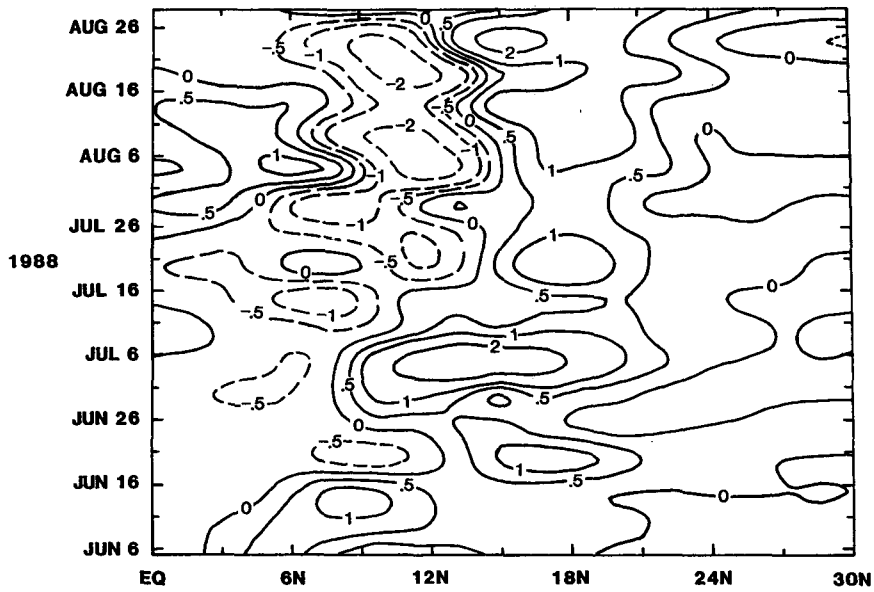

FIG. 3. Time variation of rainfall difference (afforestation − control) (mm/day) zonally averaged over the African continent. Contours are −4, −2, −1, −0.5, 0, 0.5, 1, 2, and 4 mm/day.

ally averaged over the African continent based upon 5-day rainfall averages. During the first half month of the integration, the rainfall in experiment R was nearly unchanged in the test area but was substantially increased to the south of that region. Rainfall increased in extent and intensity during late June and early July, with the maximum increase being more than 2 mm/day. After that, the positive rainfall anomaly persisted in the test area but with less intensity, about 1 mm/day. Meanwhile, the negative rainfall anomaly to the south of the test area persisted during the last two months of the integration. From Fig. 2 we can see that the decrease near the coastal area was relatively small, and the large negative anomaly only occurred in the eastern horn area.

In order to understand both evolution of the rainfall anomaly and the possible role of atmosphere–land interaction, the variations of other physical components have to be investigated. Surface evaporation and moisture flux convergence are two major moisture sources for the Sahel during the summer. In SSiB, the surface evaporation is controlled by the available energy at the surface and surface resistances, which include aerodynamic resistances, stomatal resistance, and soil resistance. After afforestation, high surface roughness, low stomatal resistance, high leaf area index, and a large water reservoir created an environment that could potentially produce high evaporation rates. Figure 4 shows the time series of the latent heat flux differences between experiments R and C. During the first half-month evaporation increased slightly in the test area. The positive anomaly spread during the second half of the first month. The increase in evaporation rate was particularly pronounced during the second and the third month. The increased rainfall apparently contributed to this change. To the south of the test area the changes in evaporation were quite small. The rainfall variation in that area was apparently caused by changes in dynamical convergence.

Figure 5 is the time series of surface temperature changes. The top soil temperature was predicted in the model using a force–restore method, which depends on the surface energy balance. During the first month of integration, the surface temperature increased in the afforestation experiment due to the reduction of surface albedo and the increase of absorbed shortwave radiation over that area. Meanwhile, the evaporation rate changed little, as shown in Fig. 4. The net gain of surface energy led to higher surface temperatures (Fig. 5) and higher sensible heat fluxes. Dry convection in the test area was quite strong and deep. Above the test area, the air temperature became warm throughout the depth of the troposphere (not shown). This enhanced vertical motion and convergence. However, since the test area was relatively dry, the moisture flux convergence was not large enough to enhance the rainfall. In addition, the higher temperatures tended to lower the relative humidity. There was a turning point in early July when the surface evaporation rate increased significantly over the whole test area and the surface temperature and low-level air temperature in the afforestation experiment were reduced. The cool temperatures below 700 mb no longer supported the thermally induced moisture convergence near the coastal area. The 3-month mean difference of moisture flux convergence (Fig. 6) was positive only in the central region of the test area and

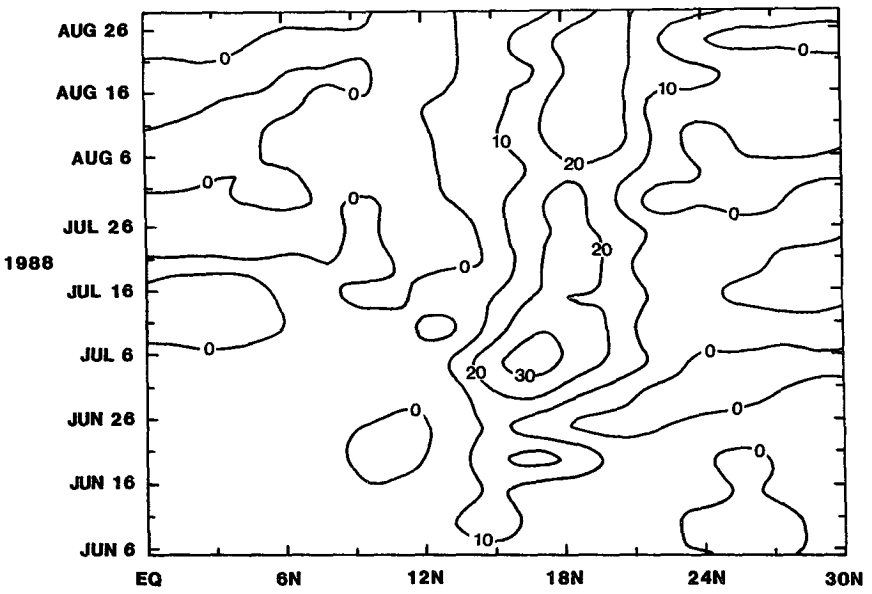

FIG. 4. Time variation of latent heat flux difference (afforestation − control) (W m^{-2}) zonally averaged over the African continent. Contour interval is 10 W m^{-2}.

negative to the south of that region. In the COLA GCM, the moisture flux convergence is closely related to the precipitation. Penetrative convection is simulated following Kuo (1965) with modification as described be Sela (1980). Convection occurs in the presence of large-scale moisture convergence accompanied by a moist unstable lapse rate under moderately high relative humidity conditions. The anomaly patterns in Fig. 6 are very consistent with those in Fig. 2. The 3-month mean moisture flux convergence increased by 0.4 mm/day, averaged over the test area, which was about 25% of the moisture flux convergence in experiment C.

The results discussed above show that land surface changes caused the circulation changes that led to changes in rainfall. The African easterly jet (AEJ) at 700–600 mb is an important feature of the atmospheric

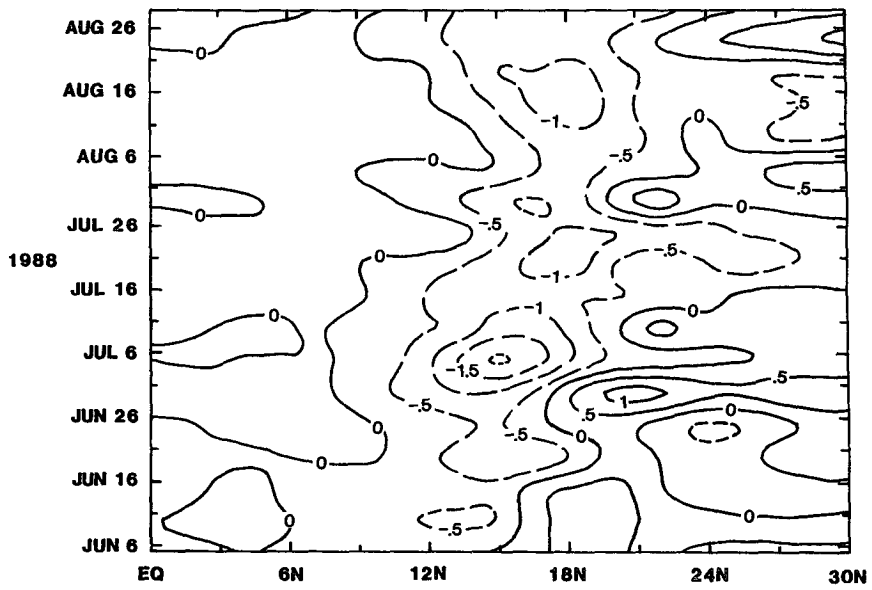

FIG. 5. Time variation of surface temperature difference (afforestation − control) zonally averaged over the African continent. Contour interval is 0.5 K.

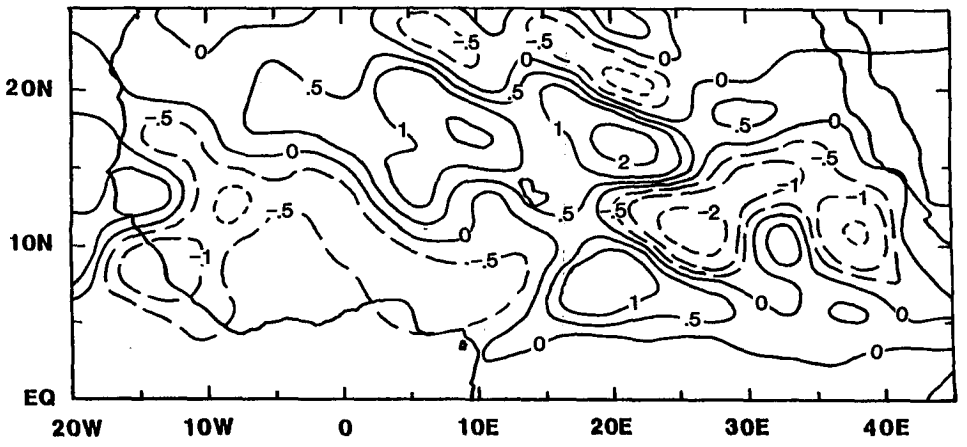

FIG. 6. Three-month mean moisture flux convergence difference (afforestation − control). Contours are −8, −4, −2, −1, −0.5, 0, 0.5, 1, 2, 4, and 8 mm/day.

circulation in this region and is very relevant to rainfall variation in the Sahel. Studies have shown that the AEJ is strong (weak) during dry (wet) years. In the upper troposphere, the tropical easterly jet (TEJ) tends to be weaker during deficient as opposed to more abundant Sahelian rainy seasons (Newell and Kidson 1984). In experiment R, the simulated AEJ was weak and the TEJ was strong, which confirmed the close relationship between the Sahel rainfall and the two easterly wind maxima. Analyses from observational data show that the rainfall reduction (increase) is associated with southward (northward) displacement of the confluence region between the northeast trades and the southwest monsoonal flow. (Lamb 1978; Lamb and Peppler 1991). The influence of changing the wind field on moisture flux can be clearly seen in Figs. 7a, and 7b,

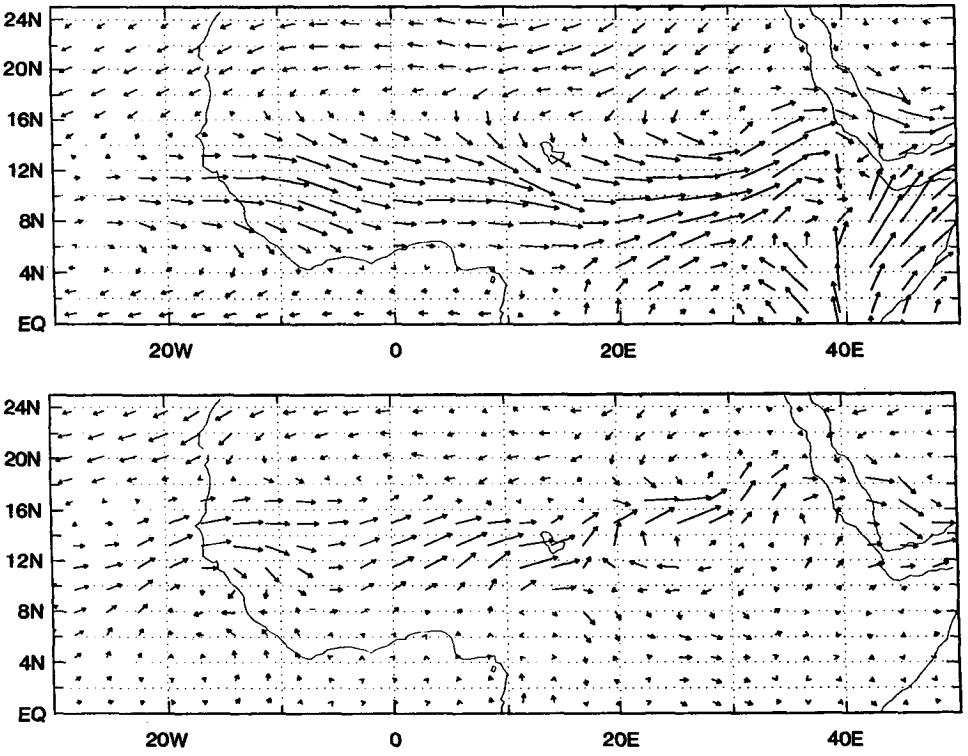

FIG. 7. July and August mean moisture flux (g kg^{-1} m s^{-1}): (a) control and (b) experiment R minus experiment C.

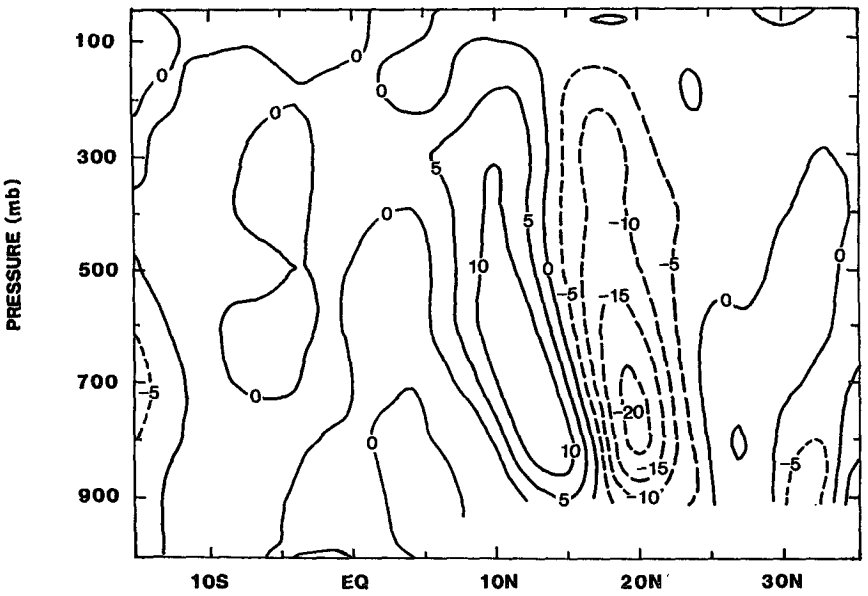

FIG. 8. Zonal averaged vertical velocity over the Africa continent for the July and August mean (afforestation − control). Contour interval is 10^{-5} mb s^{-1}.

which show the July and August mean moisture flux at 850 mb for experiment C and the difference between experiments R and C. We used 2-month means here to more clearly identify the impact of the wind field change on moisture flux convergence. Figure 7a shows that water vapor from the Atlantic Ocean is the major moisture source for the sub-Saharan area during summer months. This flow was enhanced in experiment R and created a moisture flux convergence there (see Fig. 6). The situation at 800 mb and 700 mb were very similar.

Consistent with the horizontal wind field changes, the rising motion in the test area was enhanced. Vertical motion was increased by about 30% in experiment R, especially below 600 mb (Fig. 8). This change is consistent with the increase in moisture flux convergence in this region (Fig. 6). Meanwhile, changes of the opposite sign appeared in adjacent areas, consistent with rainfall reduction there.

4. The effects of afforestation on the surface energy budget

Land surface changes modulate the surface energy balance. The vegetation canopies in the model affect the atmosphere through surface albedo, surface rough-

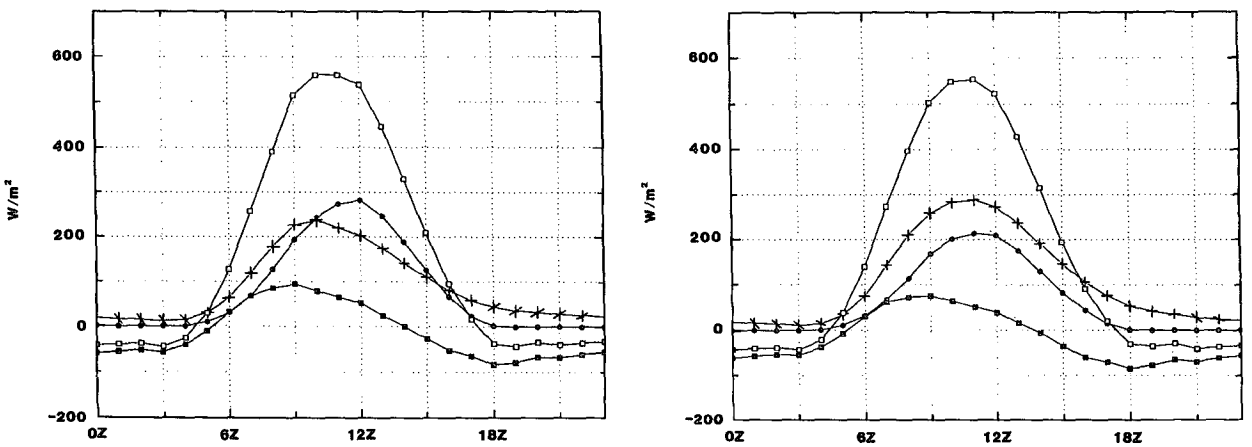

FIG. 9. August surface energy balance (W m^{-2}) for (a) control experiment (b) afforestation experiment. solid square: soil heat flux, solid circle: sensible heat, open square: net radiation at surface, and crosses: latent heat.

ness, and surface resistances, including aerodynamic resistances and stomatal resistance. In the afforestation experiment, albedo and stomatal resistance were lower, and surface roughness was higher. This increased the absorbed shortwave radiation at the surface and changed the partitioning of energy between different components. Figures 9a and 9b show the diurnal variation of the surface energy balance in August for the means of four grid points in the afforestation area in cases R3 and C3, respectively. The locations of these points are shown in Table 3.

TABLE 3. Geographic location of grid points.

Locations	Longitude	Latitude
Valley of Tilemsi, Mali	0°	18.44°N
Bou Naga, Mauritania	14.1°W	18.44°N
Guereda, Chad	22.5°E	14.93°N
Ar Raha, Sudan	30.9°E	13.17°N

The maximum latent heat flux increased by about 70 W m^{-2} and the maximum sensible heat flux was reduced by about 80 W m^{-2} in R3 at these four locations. Wallace et al. (1991) and Gash et al. (1991) have presented some measurements of available energy, evaporation, and sensible heat flux from contrasting Sahelian land types: fallow savannah and degraded forest with bare soil at Sadore, Niger (13°15′N, 2°17′E). Due to season and location differences, we are not able to directly compare their dataset with this model simulation. However, simulated changes in maximum sensible heat flux and latent heat flux between R3 and C3 have the same signs and are in the same range as those observed between fallow savannah and degraded land. Meanwhile, the differences of simulated net radiation between experiments R and C were not as large as those observed at Sadore. Increased absorbed radiation was compensated by a reduction in downward shortwave radiation due to increased cloud cover in the model.

The simulated diurnal temperature range in the Sahara desert in the current model with interactive clouds is quite realistic (about 30 K) compared to an earlier version of our model with prescribed clouds (Sato et al. 1989) because the fixed mean clouds in the previous model reduced the amount of nocturnal cooling over the desert. In experiment R the simulated mean surface air temperature in the test area was lower than in experiment C. Higher evaporation rates and a larger heat capacity in the afforestation experiment resulted in lower surface temperature. Although the average surface air temperature T_a in R was reduced by less than 1 K, this reduction was not evenly distributed during the day. For example, the daily maximum temperatures in case R3 were 2 K lower than those obtained in case C3. Meanwhile, the minimum temperatures at night did not change much. This result is consistent with other similar studies (e.g., Dickinson and Henderson-Sellers 1988). The difference between maximum and minimum temperatures in C3 is about 14 K, which is 2 K more than those observed at Sadore in September (Gash et al. 1991).

The time series of different surface energy components for experiments C and R are shown in Fig. 10. The values in these figures are the averages over the test area and are based on 5-day means. Except for sensible heat flux, the changes of other components in experiment R were consistent during the whole integration period. The 3-month mean absorbed solar radiation at the surface (Fig. 10a) was 8 W m^{-2} more over the test area due to low surface albedo, although higher cloud cover (Fig. 10b) reduced the downward solar radiation flux by about 15 W m^{-2} (Fig. 10c).

In the afforestation experiment, the moisture convergence was increased, especially in the lower troposphere (not shown). Relative humidity and cloud cover were also increased. High cloud cover caused downward longwave radiation to increase by 7 W m^{-2} (Fig. 10d). However, since the land surface change (e.g., reduced stomatal resistance) enhanced the latent heat release (Fig. 10e), the net longwave radiation at the surface was reduced by 11 W m^{-2} (Fig. 10g). The variation of net outgoing radiation flux at the top of the atmosphere was very similar to that of longwave radiation at the surface and was reduced by 9 W m^{-2} (not shown). The increased solar radiation and reduced longwave emission at the vegetated land surface was compensated by changes in sensible and latent heat fluxes. As demonstrated in many land surface studies, the high (low) surface resistances led to a low (high) evaporation rate. The latent heat flux increased persistently over the whole test area by 14 W m^{-2} (Fig. 10e). Major increases occurred during the last two months, as previously discussed. The direct re-evaporation from wet vegetated surfaces contributed 60% of this increase. During the last month, 85% of the evaporation increase was from interception loss. The sensible heat flux increased by 7 W m^{-2} in experiment R (Fig. 10f). Figure 10f shows that the largest increase occurred mainly during the first 30 days, while the gain of net solar radiation was mainly converted to sensible heat flux with little change in latent heat flux. The changes in sensible heat flux were almost identical to those of the net shortwave radiation during that time period. After 30 days, the variations of the sensible heat flux and net shortwave radiation at the surface were still highly correlated. However, the magnitude of the sensible heat flux change was lower. A comparable portion of the shortwave radiation flux was converted to latent heat flux. In the northern part of the test area, where the albedo had been reduced and absorbed shortwave radiation was increased, the sensible heat flux was higher by about 14 W m^{-2} during the last two months. In the southern part of the test area the sensible heat flux was reduced, which lowered the total increase in the test area. The soil heat flux was reduced by 2 W m^{-2} (Fig.

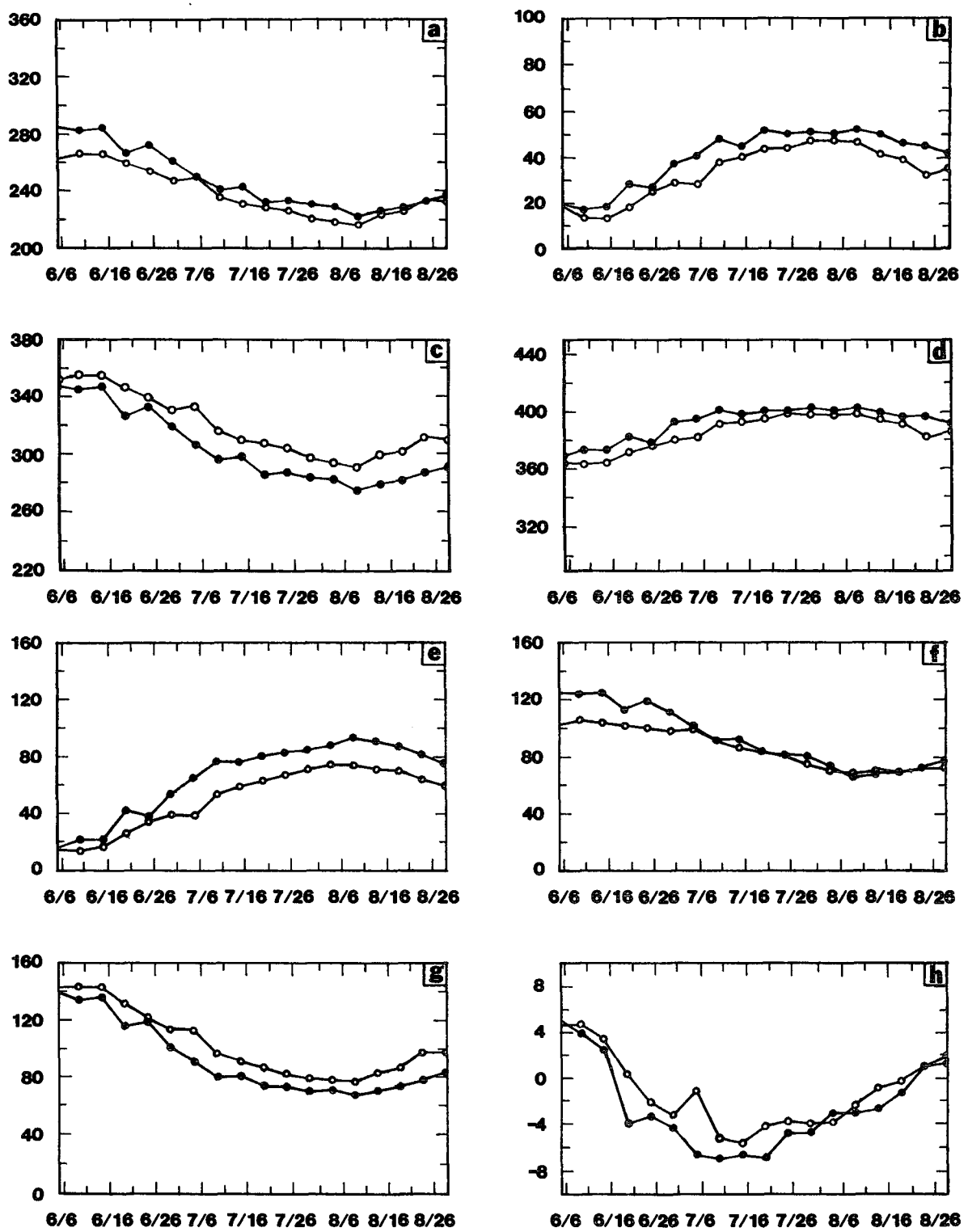

FIG. 10. Time series averaged over the test area for control experiment (open circle) and afforestation experiment (closed circle) for (a) absorbed shortwave radiation at the surface, (b) cloud cover, (c) downward shortwave radiation at the surface, (d) downward longwave radiation at the surface, (e) latent heat flux, (f) sensible heat flux, (g) net longwave radiation at the surface, and (h) soil heat flux. Units are percent for cloud cover and watts per square meter for all fluxes.

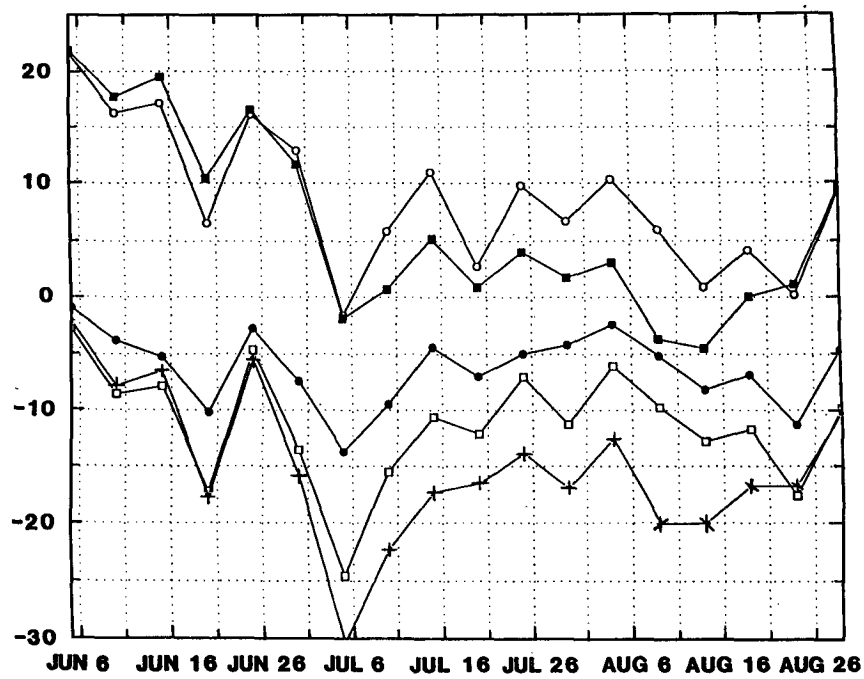

FIG. 11. Time series of the 5-day-mean differences (afforestation − control). Open circle: shortwave radiation at the surface; solid square: sensible heat; solid circle: cloud cover; open square: net longwave at the surface; and crosses: latent heat.

10h), which led to lower temperatures in experiment R. The 3-month mean surface soil wetness increased by 0.13 over the test area, which was larger than the difference in initial soil wetness.

To more clearly see the relationship among these energy components, time series of the differences of these components between experiments R and C based on 5-day means are shown in Fig. 11. The unit for energy fluxes is watts per square meter and for cloud cover is in percent. The lines for shortwave radiation, sensible heat flux, and net longwave radiation were obtained by taking the differences between the afforestation and control experiments. Because other differences, such as cloud cover and latent heat flux, had opposite phases, Fig. 11 shows these differences between the control and afforestation experiments. Changes of all these components were quite consistent throughout the period. The magnitude of the variations increased significantly late in the first month and early in the second month when temperature anomalies in the test area changed from positive to negative. This figure exhibits remarkably close correlations among the variations of these components. The correlation coefficients between the absorbed shortwave radiation and each of these components are listed in Table 4. It is clear that all of these components are highly correlated with the shortwave radiation absorbed at the surface. Since surface albedo and cloud cover directly influence the change in absorbed solar flux at the surface, the prescribed changes in surface albedo and parameterization of cloud cover may be crucial to the study of land surface–atmosphere interaction.

5. Discussion

From the results in the previous two sections, it is apparent that afforestation plays a role beyond that conventionally recognized, for example, preventing degradation of soil properties. Afforestation can also influence climate by modifying the atmospheric circulation, which then modifies rainfall. In the last two sections we focused on the results from the five case means. To

TABLE 4. Correlation coefficients of different components to absorbed shortwave radiation.

	Cloud cover	Net IR at surface	Sensible heat flux	Latent heat flux	IR out at top
Correlation coefficient	−0.79	0.86	0.86	−0.83	0.84

ensure their reliability, we compared the anomaly pattern in Fig. 2 with each pair of afforestation and control cases and found that they were very similar. All five cases had a positive anomaly in the test area and negative anomalies to the south. Only location of the maximum positive rainfall anomaly differed slightly.

As discussed earlier, our main interest here is not to investigate the effects of changes in SSTs. We used three different SSTs (climatology SST, 1950 SST, and 1983 SST) only to test the impact of the land surface change under different climate conditions. Here, we will make a brief comparison of the impact of afforestation under different global SST conditions. Figure 12 shows the comparisons among all of the cases using 1 June 1988 as an initial condition but with different SSTs: 1950 SST (wet year), 1983 SST (dry year), and climatological SST. The numbers in this figure are cumulative rainfall averaged over the test area. Case C5 (1950 SST, wet year) had the highest rainfall and C4 (1983 SST dry year) had the lowest among the three control integrations. These results are in line with the Folland et al. (1991) study, in which they used four-year SSTs to predict the Sahel rainfall, although the magnitude of the rainfall changes are not as dramatic. The differences between case C5 relative to C1 and C4 relative to C1 were about 0.5 mm/day and −0.8 mm/day, respectively. These anomalies are smaller than those observed in this region for 1950 and 1983, which were 0.8 mm/day and −1.3 mm/day, respectively (Nicholson 1985). In all three cases, rainfall increased after afforestation. However, the rainfall in case R4 (dry year SST) had the largest increase, about 1 mm/day, and was even slightly larger than that obtained in case C1, which corresponded to a normal year. For R5 (wet year SST) the rainfall increase was less, only 0.6 mm/day. The results suggest that a dry year may have a larger increase in rainfall due to afforestation. The results for the other two control runs and afforestation runs fell between cases C4 and C5 and R4 and R5, respectively (not shown). In the test area, even the lowest rainfall of the afforestation cases is higher than the highest rainfall in the control cases. This again shows that the differences between experiments R and C are significant.

We recognize that large changes in the initial soil moisture might produce significant changes in model simulation. However, in this study, our primary focus was on the impact of changes in vegetation and soil type. To test the influence of differences in initial soil moisture alone in experiments R and C, we conducted a pair of additional experiments. In these experiments, we changed the initial soil moisture only in the afforestation area, as listed in the Table 2, but other land surface properties were kept unchanged. The numerical integration in these cases started from June, which was the beginning of the rainy season. The 3-month mean rainfall over the test area in this experiment showed no difference from the control case. This suggests that changes in initial soil moisture were not a primary factor in determining enhanced rainfall in the afforestation case.

In the experiments mentioned above, we changed a relatively large area and used vegetation type 6 (broadleaf trees with ground cover) to replace the types 8 (shrubs with ground cover) and 9 (shrubs with bare soil). The response apparently depended on the changes in the surface characteristics and the extent of afforestation. To test the dependency of afforestation results on the scale and degree of land surface change, we altered the surface conditions with different vegetation types and/or less afforestation area (Table 2). In case R32, we used type 2, broadleaf deciduous trees, to replace the semidesert area. This type of vegetation can be found sporadically in the southern Sahel and Gulf of Guinea region. The average surface albedo for this type was about 0.14, about 0.16 less than in type 9 and about 0.07 less than in type 8. The initial soil wetness was larger than in the control run by approximately 0.12.

Figures 13a and 13b show the 3-month rainfall anomalies for cases R3 − C3 and R32 − C3, respectively. Both cases had the same initial condition and had the same size of area afforested, but each case used different vegetation types for afforestation. Despite the high surface roughness length, much lower surface albedo, and large vegetation cover and leaf area index (both are almost 100% more than in type 6), the average rainfall over the test area in case R32 was only slightly more than in case R3. This is because, although the rainfall in case R32 significantly increased in the southern part of the test area compared with case R3, the rainfall was less than in case R3 in the northern part of the test area. The gradient in Fig. 13b near the southern boundary of the test area was larger than that in Fig. 13a. Both the positive anomaly in the southern portion of the test area and the negative anomaly to the south were enhanced. Striking differences of the rainfall anomaly between cases R32 and R3 occurred in East Africa. In contrast to experiment R, case R32 had a positive rainfall anomaly in this area (Fig. 13b). The latent heat flux in case R32 was about 10 W m^{-2} more than in case R3 in East Africa, which helped to enhance the rainfall there. However, over the entire test area the average evaporation rate in case R32 was not substantially changed as compared to case R3. Although the re-evaporation in case R32 was twice as much as in case R3, it was largely offset by the reduction of direct evaporation from the soil. The large increase of absorbed solar radiation at the surface, 22 W m^{-2}, was mainly converted to sensible heat flux, which was 29 W m^{-2} more than in case C3. The surface temperature was reduced significantly, by 1.5 K, which was 1 K lower than in case R3.

In another experiment, which includes cases RS1, RS2, and RS3 (see Table 2), we changed a small area that originally had vegetation type 8 (Fig. 14). The

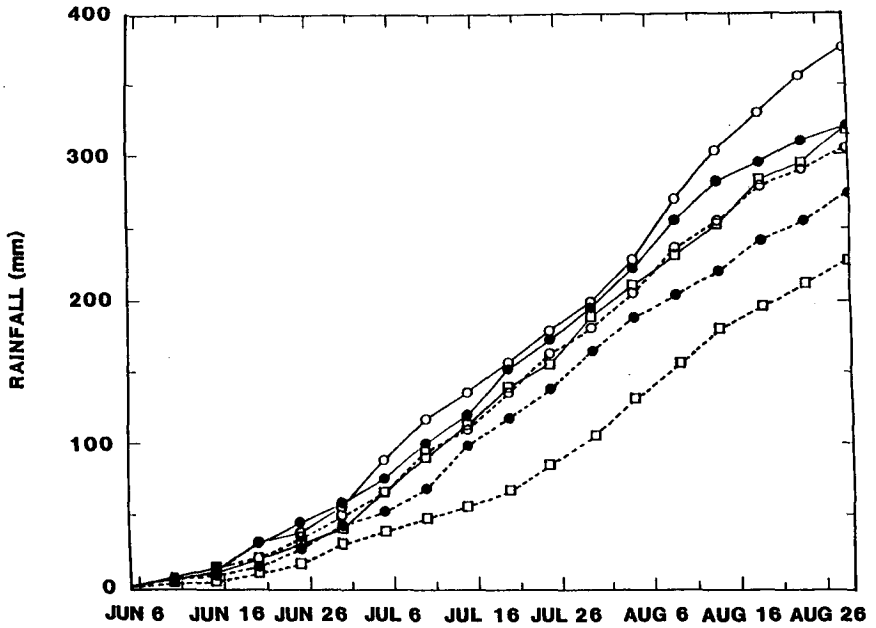

FIG. 12. Accumulated rainfall (mm) for three control cases and three afforestation cases. Open circle: case R5, dot–solid line: case R1, open square–solid line: case R4, open circle: case C5, dot–dashed line: case C1, and open square–dashed line: case C4.

average width is two grid points, or about 4°. Since the area changed is much smaller than that for experiment R, we chose type 2 for afforestation. Here, we repeated the experiment three times to control the model internal variability. We refer to the three sample means for control and afforestation experiments as experiments CS and RS, respectively. The experiment CS is the average of cases C1, C2, and C3. The 3-month mean rainfall difference between RS and CS is shown in Fig. 15. The rainfall was increased by 0.4 mm/day in the area where we changed the surface conditions. Actually, the rainfall was not substantially increased during the first month of integration. Rainfall in the last two months made major contributions to the positive anomaly. The negative rainfall anomaly area, which was located to the south of the afforestation area, was smaller than that in the experiment R. Comparing the results from experiments R, RS, and case R32, we can find that the intensity of the dipole patterns is related to the contrast of the adjacent land surface characteristics. The sharper the contrast between two adjacent areas, the stronger the intensity of the dipole pattern. The increased absorbed shortwave radiation at the surface in RS was mainly converted to sensible heat flux, which increased by 9 W m^{-2}. The temperature in the test area in experiment RS was lower by 1.2 K. This feature was quite persistent during the whole period. The evaporation rate was not significantly increased. This again confirmed our earlier results that the rainfall increase was mainly due to changes in circulation. Due to the limitations of the model resolution we are not able to further reduce the width of the afforestation belt. For the case with reduced afforestation areas, no consistent changes in the pattern of rainfall were found when vegetation type 6 was used for afforestation.

In this study the prescribed land surface parameters in the afforestation area are perturbed in the opposite direction compared to the desertification experiment described in Part I. For example, low albedo and high vegetation cover are prescribed in experiment R, whereas high surface albedo and low vegetation cover are prescribed in experiment D. The simulated rainfall anomalies for desertification and afforestation experiments are in agreement with the observed rainfall anomalies during the dry and the wet years. We find that the changes in atmospheric circulation and energy balance in experiment R are indeed opposite to those in experiment D. The most remarkable feature is the reversal of the rainfall dipole. Instead of a positive rainfall anomaly to the south of the desertification area, there was a rainfall deficit to the south of the afforestation area. Similar to the desertification experiment, the rainfall change mainly remained in the test area. Another area with relatively large rainfall change was in the western Pacific Ocean. Since climatic fluctuations over this area are large in model simulations even without any forced perturbations, we can not infer from this experiment that the anomalies there are linked to land surface property changes in the Sahel.

There are several significant differences between the desertification and the afforestation experiments. One of the differences is in the pattern of rainfall changes.

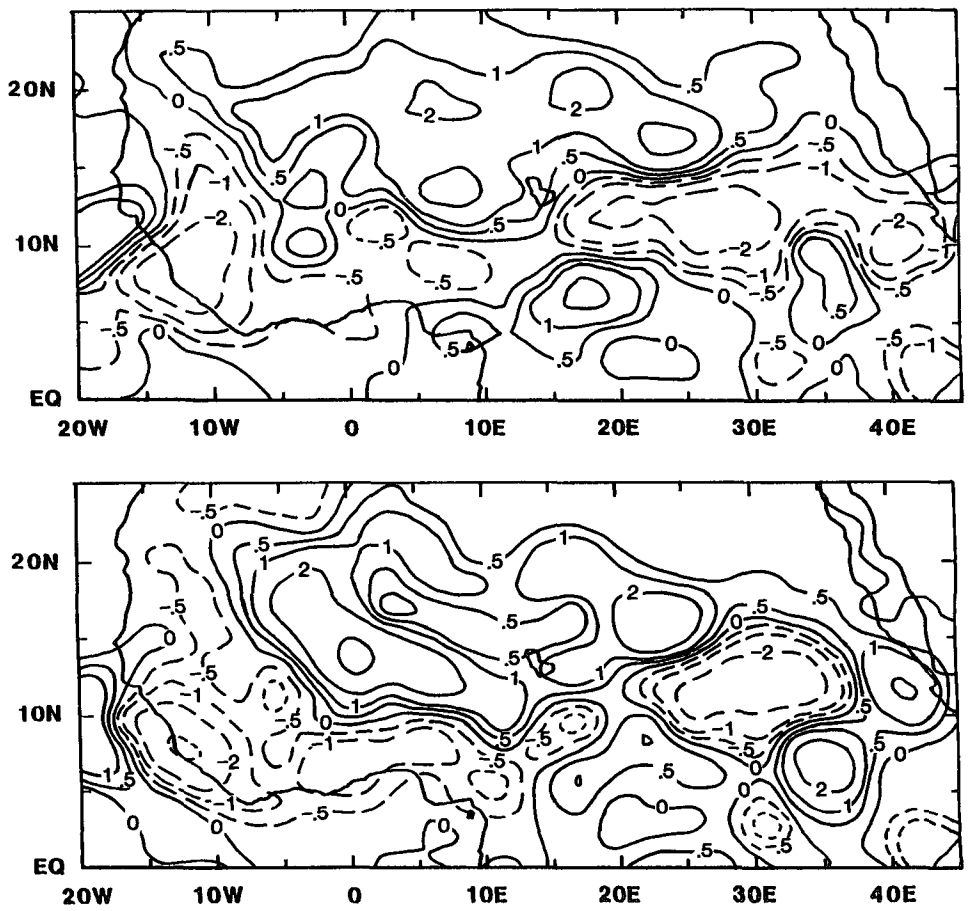

FIG. 13. Three-month mean rainfall difference. (a) R3 − C3 and (b) R32 − C3. Contours are −8, −4, −2, −1, −0.5, 0, 0.5, 1, 2, 4, and 8 mm/day.

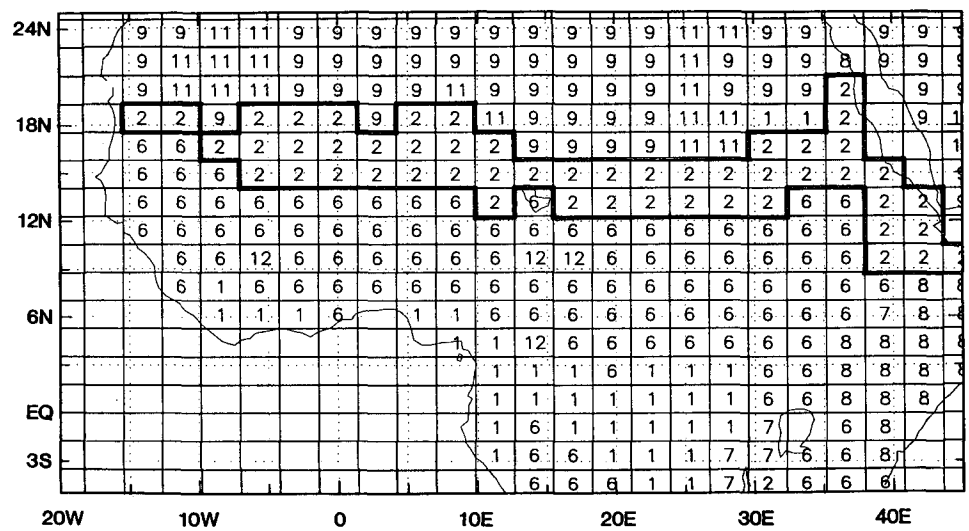

FIG. 14. Vegetation type map in the sub-Saharan region for the revised afforestation experiment RS.

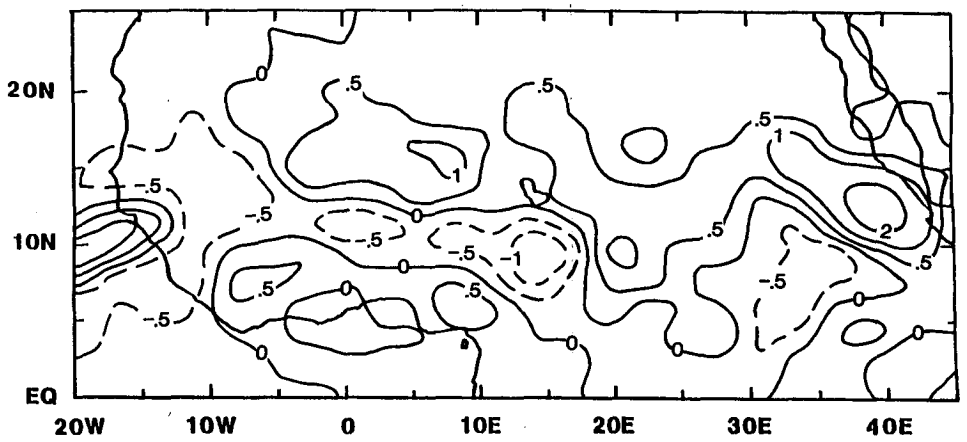

FIG. 15. Three-month mean rainfall differences between experiments, RS − CS. Contours are −8, −4, −2, −1, −0.5, 0, 0.5, 1, 2, 4, and 8 mm/day.

In the desertification experiment, a zonal rainfall anomaly pattern was found over the entire desertification area, whereas in the afforestation experiment the rainfall anomaly was located mainly in the center of the test area. The evolution of the anomalies in the afforestation experiment was also quite different from that in the desertification experiment, especially in the initial stages. In the desertification experiment, the model responded much more rapidly to the land surface change, and the anomaly persisted for the entire integration. In afforestation experiment, the evaporation, the AEJ, and in turn, the rainfall did not have significant changes in the first month. The substantial changes started in the second month. In experiment D, the rainfall deficit closely followed the prescribed desertification area. The maximum rainfall reduction was in West Africa. In contrast, not all of the test area had positive rainfall anomalies in experiment R. The rainfall was significantly increased in the central part of the sub-Saharan area. Meanwhile, there was a southward shift of the axis of maximum rainfall in the desertification experiment and no such shift in the afforestation experiment. The above comparisons suggest that the response to changes in land surface properties is not linear and that the climate in the Sahel is especially vulnerable to the nature and location of the land surface perturbation because the Sahel region is near the edge of the subsidence branch of the Hadley circulation. The afforestation area that we chose is located to the north of the desertification area, where the subsidence is even stronger.

6. Summary

This hypothetical study suggests that large-scale afforestation in the sub-Saharan area could help to enhance the rainfall in that region. The rainfall in experiment R was significantly different from that in the control experiment. While the rainfall increased in the afforestation region, model results showed a reduction in rainfall to the south of this region. Among five cases, the case using 1950 SST had the highest rainfall and the case using 1983 SST had lowest rainfall in the Sahel, consistent with other empirical investigations and numerical experiments about the effect of SST on the Sahel climate. Afforestation had the largest impact during the simulation of a dry year. Reducing the afforestation area by roughly 50% still resulted in increased simulated rainfall. The anomaly evolution process in this experiment showed that the land surface change induced a change in temperature and circulation, which in turn led to the rainfall change. The surface energy balance analysis showed that the surface albedo and cloud cover are two very important factors controlling the changes in land surface–atmosphere interaction. A possible limitation of the present study is that the model was integrated only up to a season. Similar experiments should be considered with long-term integrations of realistic climate models. We also suggest that similar experiments be carried out using other climate models with different parameterizations of convection, boundary layer, and land surface processes.

This is only a sensitivity study of the potential climatic impact of afforestation in the Sahel region and does not address any social, economical, or technical factors related to the planting and maintenance of trees. However, while designing this experiment we did consider some relevant issues. For example, the vegetation type 6 that we selected for afforestation can be found in nearby areas at a similar latitude, which would avoid the adverse effects due to a different climate (Goor and Barney 1968). However, this experiment should be considered only as a first step toward more realistic assessments of the effect of afforestation on the Sahel climate. In particular, more research with additional models using long-term integrations is needed to determine the locations and impact of sustainable afforestation in the sub-Sahara region.

Acknowledgments. This research was supported by NASA Grants NAGW-1269, NAGW-557, and NSF ATM-9019296. We wish to thank Dr. James Kinter, Dr. Heidi Basetable, and Mike Fennessy for their helpful comments and suggestions on this paper. We would like to extend our gratitude to Drs. P. Sellers and D. Straus for their helpful discussions during this research work. Dr. P. Lamb provided useful materials to support our desertification and afforestation studies and gave detailed comments on this paper. We appreciate comments by Dr. Lamb and other reviewers. Special thanks go to Tammy Yeargin for her editorial assistance.

REFERENCES

Anthes, R. A., 1984: Enhancement of convective precipitation by mesoscale variations in vegetative covering in semiarid regions. *J. Climate Appl. Meteor.*, **23,** 541–554.

Black, J. F., and B. Tarmy, 1963: The use of asphalt coatings to increase rainfall. *J. Appl. Meteor.*, **2,** 557–564.

Charney, J. G., 1975: Dynamics of deserts and drought in the Sahel. *Quart. J. Roy. Meteor. Soc.*, **101,** 193–202.

Dickinson, R. E., and A. Henderson-Sellers, 1988: Modelling tropical deforestation: A study of GCM land-surface parameterizations. *Quart. J. Roy. Meteor. Soc.*, **114,** 439–462.

Dorman, J. L., and P. J. Sellers, 1989: A global climatology of albedo, roughness length, and stomatal resistance for atmospheric general circulation models as represented by the Simple Biosphere Model (SiB). *J. Appl. Meteor.*, **28,** 833–855.

Flohn, H., D. Henning, and H. C. Korff, 1974: Possibilities and limitations of a large-scale water budget modification in the Sudan–Sahel belt of Africa. *Meteor. Rundsch.*, **27,** 100–109.

Food and Agriculture Organization of the United Nations (FAO), 1989: Role of forestry in combating desertification. *FAO Conservation Guide,* Vol. 21, 331 pp.

Folland, C. K., T. N. Palmer, and D. E. Parker, 1986: Sahel rainfall and worldwide sea temperatures. *Nature,* **320,** 602–607.

——, J. Owen, M. N. Ward, and A. Colman, 1991: Prediction of seasonal rainfall in the Sahel region using empirical and dynamical methods. *J. Forecasting,* **1,** 21–56.

Gash, J. H. C., J. S. Wallace, C. R. Lloyd, A. J. Dolman, M. V. K. Sivakumar, and C. Renard, 1991: Measurements of evaporation from fallow Sahelian savannah at the start of the dry season. *Quart. J. Roy. Meteor. Soc.*, **117,** 749–760.

Glantz, M. H., 1977: Climate and weather modification in and around arid lands in Africa. *Desertification,* M. H. Glantz, Ed., Westview Press, 307–338.

Goor, A. Y., and C. W. Barney, 1968: *Forest Tree Planting in Arid Zones.* The Ronald Press, 409 pp.

Kuo, H. L., 1965: On formation and intensification of tropical cyclones through latent heat release by cumulus convection. *J. Atmos. Sci.*, **22,** 40–63.

Lamb, P. J., 1978: Large-scale tropical Atlantic surface circulation patterns associated with sub-Saharan weather anomalies. *Tellus,* **30,** 240–251.

——, and R. A. Peppler, 1991: West Africa. *Teleconnections Linking Worldwide Climate Anomalies,* M. Glantz, R. W. Katz, and N. Nicholls, Eds., Cambridge University Press, 121–189.

Le Houerou, H. N., 1977: The nature and causes of desertification. *Desertification,* M. H. Glantz, Ed., Westview Press, 17–38.

Mintz, Y., and Y. V. Serafini, 1984: Global fields of monthly normal soil moisture as derived from observed precipitation and estimated potential evapotranspiration. Land surface influences on weather and climate. F. Baer and Y. Mintz, Eds., Final Tech. Report, NASA-CR-173575, 182 pp.

Newell, R. E., and J. W. Kidson, 1984: African mean wind changes between Sahelian wet and dry periods. *J. Climatol.*, **4,** 27–33.

Nicholson, S. E., 1985: Sub-Sahara rainfall 1981–1984. *J. Climate Appl. Meteor.*, **24,** 1388–1391.

Sato, N., P. J. Sellers, D. A. Randall, E. K. Schneider, J. Shukla, J. L. Kinter III, Y.-T. Hou, and E. Albertazzi, 1989: Implementing the simple biosphere model (SiB) in a general circulation model: Methodologies and results. NASA Contractor Rep. 185509, 76 pp.

Sela, J. G., 1980: Spectral modeling at the National Meteorological Center. *Mon. Wea. Rev.*, **108,** 1279–1292.

Sellers, P. J., Y. Mintz, Y. C. Sud, and A. Dalcher, 1986: A Simple Biosphere Model (SiB) for use within general circulation models. *J. Atmos. Sci.*, **43,** 505–531.

Semazzi, F. H. M., V. Mehta, and Y. C. Sud, 1988: An investigation of the relationship between sub-Sahara rainfall and global sea surface temperatures. *Atmos.–Ocean,* **26,** 1471–1485.

Shukla, J., and Y. Mintz, 1982: Influence of land-surface evapotranspiration on the earth's climate. *Science,* **215,** 1498–1501.

Stebbing, E. P., 1938: The man-made desert in Africa. *J. Roy. African Soc.,* **37** (Suppl), 13.

Wallace, J. S., I. R. Wright, J. B. Stewart, and C. J. Holwill, 1991: The Sahelian energy balance experiment (SEBEX): Ground based measurements and their potential for spatial extrapolation using satellite data. *Adv. Space Res.,* **11**(3), 131–141.

Xue, Y., and J. Shukla, 1993: A numerical experiment to study the influence of changes in the land surface properties on Sahel climate. Part I: Desertification. *J. Climate,* **6,** 2232–2245.

——, K. N. Liou, and A. Kasahara, 1990: Investigation of biogeophysical feedback on the African climate using a two-dimensional model. *J. Climate,* **3,** 337–352.

——, P. J. Sellers, J. L. Kinter III, and J. Shukla, 1991: A simplified biosphere model for global climate studies. *J. Climate,* **4,** 345–364.